frontiers | Frontiers in Earth Science

BRIEF RESEARCH REPORT
published: 21 June 2022
doi: 10.3389/feart.2022.903743

Investigation Into Deformation and Failure Characteristics of the Soft-Hard Interbedded Rock Mass Under Multiaxial Compression

Ang Li[1], Guojian Shao[2], Yaodong Li[3], Yang Sun[4], Jingbo Su[5] and Juncheng Liu[6]*

[1]College of Harbour, Coastal and Offshore Engineering, Hohai University, Nanjing, China, [2]College of Mechanics and Materials, Hohai University, Nanjing, China, [3]College of Mechanics and Materials, Hohai University, Nanjing, China, [4]College of Harbour, Coastal and Offshore Engineering, Hohai University, Nanjing, China, [5]College of Harbour, Coastal and Offshore Engineering, Hohai University, Nanjing, China, [6]Pumped-storage Technology and Economic Research Institute State Grid Xin Yuan Company Ltd., Beijing, China

The influence of loading path, intermediate principal stress and weak layers on the deformation property and failure characteristics of soft-hard interbedded rock mass is initially discussed in this study. First, the laboratory experiments of multiaxial compression failure are carried out to soft-hard interbedded rock samples of Jinping. Three failure modes of rock samples caused by different distribution forms of weak layers under uniaxial compression and deformation property and failure characteristics of rock samples in different loading paths under biaxial compression are analyzed. Then, considering the property of strain softening, numerical models are established based on the elastic-brittle-plastic constitutive relation. The effect of weak layer dip angle, quantity, distribution form, and volume ratio on strength characteristics is further investigated. The results reveal that the failure mode of Jinping soft-hard interbedded rock samples generally follows the pattern of multi-fracture splitting under uniaxial compression, and the pattern of tension-shear damage under biaxial compression. The intermediate principal stress is positively correlated with the vertical failure loading. The number of weak layers has no significant effect on the "U" type strength characteristics of samples. However, as the number of weak layers increases, there is a tendency for the minimum of vertical failure loading to move forward in the direction of smaller dip.

Keywords: hydro-junction project of JinPing, soft-hard interbedded rock mass, multiaxial compression experiment, numerical simulation, elastic-brittle-plastic constitutive relation

OPEN ACCESS

Edited by:
Chaojun Jia,
Central South University, China

Reviewed by:
Xianze Cui,
China Three Gorges University, China
Shengxin Zhu,
Beijing Institute of Technology, China

****Correspondence:***
Ang Li
liang2008@hhu.edu.cn

Specialty section:
This article was submitted to Structural Geology and Tectonics, a section of the journal Frontiers in Earth Science

Received: *24 March 2022*
Accepted: *29 April 2022*
Published: *21 June 2022*

Citation:
Li A, Shao G, Li Y, Sun Y, Su J and Liu J (2022) Investigation Into Deformation and Failure Characteristics of the Soft-Hard Interbedded Rock Mass Under Multiaxial Compression. Front. Earth Sci. 10:903743. doi: 10.3389/feart.2022.903743

1 INTRODUCTION

The soft-hard interbedded rock mass, as a special structural rock mass, is widely found in nature. Because of its deformation transverse isotropy and strength anisotropy, but also by the influence of the soft and hard components, the mechanical property is very complex, which has attracted a great deal of interest (Brady et al., 2004).

In the past decades, the soft-hard interbedded rock mass has mostly been simplified to the transverse isotropic rock mass like stratified rock mass at macroscopic level. Also, the mechanical property of both nature and synthetic transverse isotropic rocks has been investigated (Niandou et al., 1997; Tien et al., 2000; Tien et al., 2006; Lu et al., 2009; Li et al., 2014; Wang et al., 2018; Shen et al., 2021). On one hand, the

shape of the curve relating to compression strength and dip angle under varied confining pressure is an important representation of the research. It found that most transverse isotropic rocks have their maximal compression strength at an dip angle 0° or 90°, and their minimal compression strength at an dip angle in the range of 30°–45°. With increase of confining pressure, the rock mass become more ductile, and the effect of the strength anisotropy is usually reduced. It has also been studied in terms of influence factors such as the way layers are assembled, and the composition of the rock formation on the strength, deformation characteristics, and damage patterns of stratified rock mass. For example, based on analysis of field surveys, Chen et al. (2000) classified the structure characteristics of stratified rock mass and proposed "the sample element method" to emulate the field large-size trail. Combined the effect of stress redistribution and rock structure, Yan et al. (2016) discussed the coring damage mechanism of the Yan-tang group marble containing a kind of inclined grey ribbon-like stripes. Considering the existence of rock structure at mesoscale, Li et al. (2018) investigated the influence of heterogeneity on mechanical property of soft-hard rock samples from the perspective of mesomechanics. But overall, there is still a lack of information on the influence of distribution pattern, and the volume ratio of the different constituent materials on the mechanical property of soft-hard interbedded rock mass.

On the other hand, several failure criteria have been proposed to predict the variation of compression strength of transversely isotropic rocks with the dip angles under various confining pressure. According to the assumption and the treatment method, they can be divided into two main categories, continuity criteria and discontinuity criteria. For continuity failure criteria, some progress has been made in its mathematical approach and empirical theory (Nova et al., 1980; Cazacu et al., 1998; Pietruszczak et al., 2002; Parisio et al., 2018). However, for the rock mass with strong discontinuity, the simulation of their anisotropic strength property by continuity criteria, and the value of relevant parameters still need to be further enhanced. For discontinuity failure criteria, the basic assumption is that the failure of the anisotropic rocks is mainly caused by the extension of laminae or fractures in the bedrock, and separate failure criteria are used for these two different failure forms. The most popular discontinuity failure criteria, called "the single plane of weakness theory", were suggested by Jaeger et al. (1960). Afterward, this theory has been further extended (Mclamore et al., 1967; Duveau et al., 1998; Tien et al., 2001; Huang et al., 2010; Xu et al., 2017; Mohamed et al., 2019). At present, the establishment of a uniform failure criterion for stratified rock mass that take into account the effect of intermediate principal stress based on true triaxial tests is a hot issue for research.

This study is a preliminary study on the mechanical properties of soft-hard interbedded rock mass of Jingping. It is structured as follows: in **section 2**, the research method is introduced, including the setup of laboratory experiments of multiaxial compression failure and the numerical simulation scheme. In **section 3**, results are discussed, including the effect of loading path and intermediate principal stress on deformation and failure characteristics of rock samples under biaxial compression and the effect of dip angle, quantity, distribution form, and volume ratio of weak layers on strength characteristics and failure pattern of rock samples under uniaxial compression. In **section 4**, some concluding remarks are presented.

2 RESEARCH METHOD

2.1 Setup of Laboratory Experiments of Multiaxial Compression Failure

2.1.1 Information of Rock Samples

The experimental rock interbedded greyish-white marble and green schist was taken from the underground caverns of Jinping Hydroelectric Station. The microstructure of the two components is shown in **Figure 1A**. The marble component is relatively hard, with a medium to fine-grained structure and calcite as the main mineral constituents. The green schist component is relatively soft, with calcite and chlorite schist as the main mineral components, and is characterized by the development of lamellar and looseness. In accordance with the relevant specification, the rock was processed into cubic rock samples with sides of 50 and 70 mm in length, where the 70-mm cubic rock samples have a dip of approximately 30°. The 50-mm cube samples were selected for experiments of uniaxial compression failure, and the 70-mm cube samples were selected for experiments of biaxial compression failure.

2.1.2 Experiment Procedure

Experiments of uniaxial compression failure were carried out on the electro-hydraulic servo uniaxial universal testing machine WAW-E2000 as shown in **Figure 1D**. The maximum loading capacity of the testing machine is 2000 kN, and the experiment of biaxial compression failure was conducted using the biaxial universal testing machine CSS-283, as shown in **Figure 1E**. The maximum loading capacity of the testing machine is 500 kN (compression), 200 kN (tension) in the vertical direction, and 300 kN (pressure) in the horizontal direction. Differential displacement sensors were used to measure the deformation with a deformation measurement range of 1 mm and a resolution of 1 μm.

In total, two types of loading path were used during the biaxial experiments:1) loading with a constant lateral pressure. In three experiment groups, the horizontal lateral pressure is first loaded to 3, 6, and 9 MPa at a rate of 2 MPa/min, respectively, and then the loading is held constant, followed by loading vertical pressure until rock samples were failed; 2) loading with a constant lateral pressure ratio followed by the constant lateral pressure. In the experiment group, vertical and horizontal pressures are first loaded simultaneously until 9 MPa according to the stress ratio of 1:1, with the loading rate both of 2 MPa/min. Then, the horizontal loading is kept constant, followed by loading the vertical pressure according to the original loading rate until rock samples were failed.

2.2 Numerical Simulation Scheme and Computational Modeling

2.2.1 Numerical Simulation Scheme

In order to further investigate the influence of dip angle, quantity, distribution, and volume ratio of weak layers on strength characteristics and failure pattern of rock samples; numerical

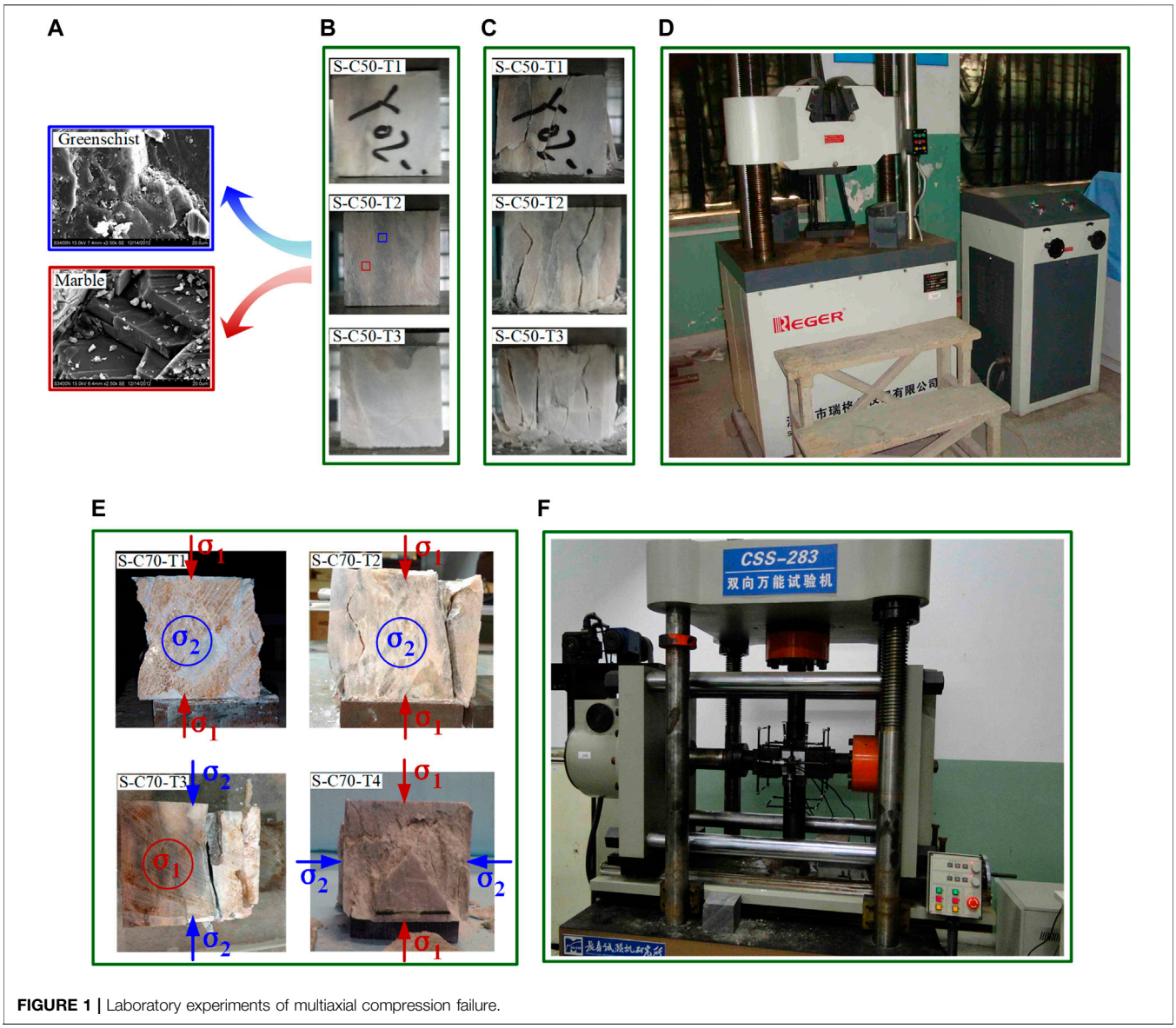

FIGURE 1 | Laboratory experiments of multiaxial compression failure.

TABLE 1 | Information of greenschist layers in each test group.

Test group name	S-1-N-β	S-1-W-β	S-2-β	S-3-β
Number of green schist layers	1	1	2	3
Volume ratio of green schist layers/%	8.52	18.92	17.04	25.56
Sketch of the test group				

simulations were used to carry out comparative compression failure tests on four groups of soft-hard interbedded rock samples (S-1-N-β, S-1-W-β, S-2-β, and S-3-β) under uniaxial compression. The dip angles of 0°, 15°, 30°, 45°, 60°, 75°, and 90° were set for each group samples. As can be seen in **Table 1**, the number of weak layers in rock sample groups S-1-N-β, S-2-β, and

TABLE 2 | Parameters of soft-hard interbedded rock mass in Jinping.

Type of rock material	Young's modulus/GPa	Poisson's ratio	Cohesion/MPa	Friction angle/°	Tensile strength/MPa
Marble	50	0.22	45	50	2
Greenchist	11	0.25	10	37	1

Note: residual tensile strength coefficient and residual cohesion coefficient defined as 0.1, respectively.

S-3-β tends to increase in succession, and for the same number of weak layer, the volume ratio of green schist in the rock sample group S-1-W-β is higher than that in the rock sample group S-1-N-β.

2.2.2 Computational Modeling

The numerical procedure was carried out using the elastic-brittle-plastic modeling based on strain softening. In this modeling, the Mohr–Coulomb yield criterion with a tensile cut-off is adopted as a criterion for the onset of element degradation. The plastic parameters κ^s and κ^t, which are closely related to the plastic shear and plastic tensile strains, are introduced and the strength parameters are expressed as a function of both to describe its plastic shear softening behavior and plastic tensile softening behavior. The incremental mathematical expression for κ^s and κ^t are as follow:

$$\Delta\kappa^s = \sqrt{\frac{\left(\Delta\varepsilon_1^{ps} - \Delta\varepsilon_m^{ps}\right)^2 + \left(\Delta\varepsilon_m^{ps}\right)^2 + \left(\Delta\varepsilon_3^{ps} - \Delta\varepsilon_m^{ps}\right)^2}{2}}, \quad (1)$$

$$\Delta\kappa^t = \Delta\varepsilon_3^{pt}, \quad (2)$$

$$\Delta\varepsilon_m^{ps} = \frac{\Delta\varepsilon_1^{ps} + \Delta\varepsilon_3^{ps}}{3}, \quad (3)$$

where $\Delta\varepsilon_1^{ps}$ and $\Delta\varepsilon_3^{ps}$ are the plastic shear strain increments in the direction of the first principal stress and the third principal stress, respectively; $\Delta\varepsilon_3^{pt}$ is the plastic tensile strain increment.

For the numerical grid, a homogenized computational grid of soft-hard interbedded rock samples is established by the proportional relationship mapping method. The grid size is 50 mm × 50 mm, with an element scale of 0.5 mm × 0.5 mm, divided into 10,000 cells in total. The relevant mechanical parameters of the Jinping soft-hard interbedded rock mass are given in **Table 2** referring to literature (Deng et al., 2001; Chengdu Hydroelectric Investion and Design Institute and China Hydropower Engineering Consulting Group Co, 2003; Huang et al., 2008). As the friction angle of brittle hard rock usually does not change much before and after failure, the effect of friction angle is not considered in the calculation.

3 RESULTS AND ANALYSIS

3.1 Experimental Results and Analysis

3.1.1 Laboratory Experiments of Uniaxial Compression Failure

Figure 1B,C show a comparison of typical rock samples before and after failure under uniaxial compression. It can be seen from the figures the rock sample S-C50-T1 consists of a simple splice of green schist with marble to the left and right, with a dip angle of 0°. When the axial compression reaches 191.2 kN, the sample is failed with significant brittleness. The final main crack of failure occurs within each of the soft and hard rock layers near the junction and at an angle to the loading direction. The rock sample S-C50-T2 has weak layers of green schist on the left, middle and right sides, with the left and middle layer at a dip angle of 0° and a through trend in the middle layer. In contrast, the right layer is thinner and at an angle to the loading direction. When the axial compression reaches 143.3 kN, the sample is failed. The failure pattern is characterized by penetration failure in the left and middle layers of the green schist and main cracking failure from the expansion of the thin layer on the right side. The expansion trend of the main crack is highly correlated with the distribution of the thin layer of the green schist. The layers of green schist in rock sample S-C50-T3 are mainly present in the left and upper sides, with a relatively concentrated distribution. When the axial compression reaches 339.7 kN, through main crack occurred on the left layers of green schist at an angle to the loading direction. At the same time, multiple cracks along the loading direction appear inside the layer of green schist in the upper side at an angle of 90° to the loading direction. The sample eventually maintains a typical failure form of multi-fracture split under uniaxial compression.

In general, it can be seen from the experiments that the failure characteristics of the soft-hard interbedded rock mass of Jinping are closely related to the dip angle of weak layer, and the failure mode basically follows the multi-fracture split mode of uniaxial compression failure. The specific failure mechanism is in good agreement with the single weak face theory developed by Jaeger (Jaeger et al., 1960; Tien et al., 2001; Mohamed et al., 2019), that is in the range of slow dip angle, the failure of rock mass is controlled by the property of the rock material itself while in the range of larger dip angle the influence of weak structural surfaces is the dominant factor.

3.1.2 Laboratory Experiments of Biaxial Compression Failure

Figure 2 shows the typical stress, strain and time curves of 70 mm cubic rock samples in different loading paths under biaxial compression. As can be seen, the second principal strain is significantly smaller than the first principal strain for both loading paths and undergoes a positive to negative variation. At higher stress (σ_2 = 6 MPa, 9 MPa), the slope of the strain-time curve increases and has an upward trend as the rock sample approaches failure. In the constant lateral compression loading path, the failure strength increases from 73.50 MPa, 77.96–82.65 MPa as the

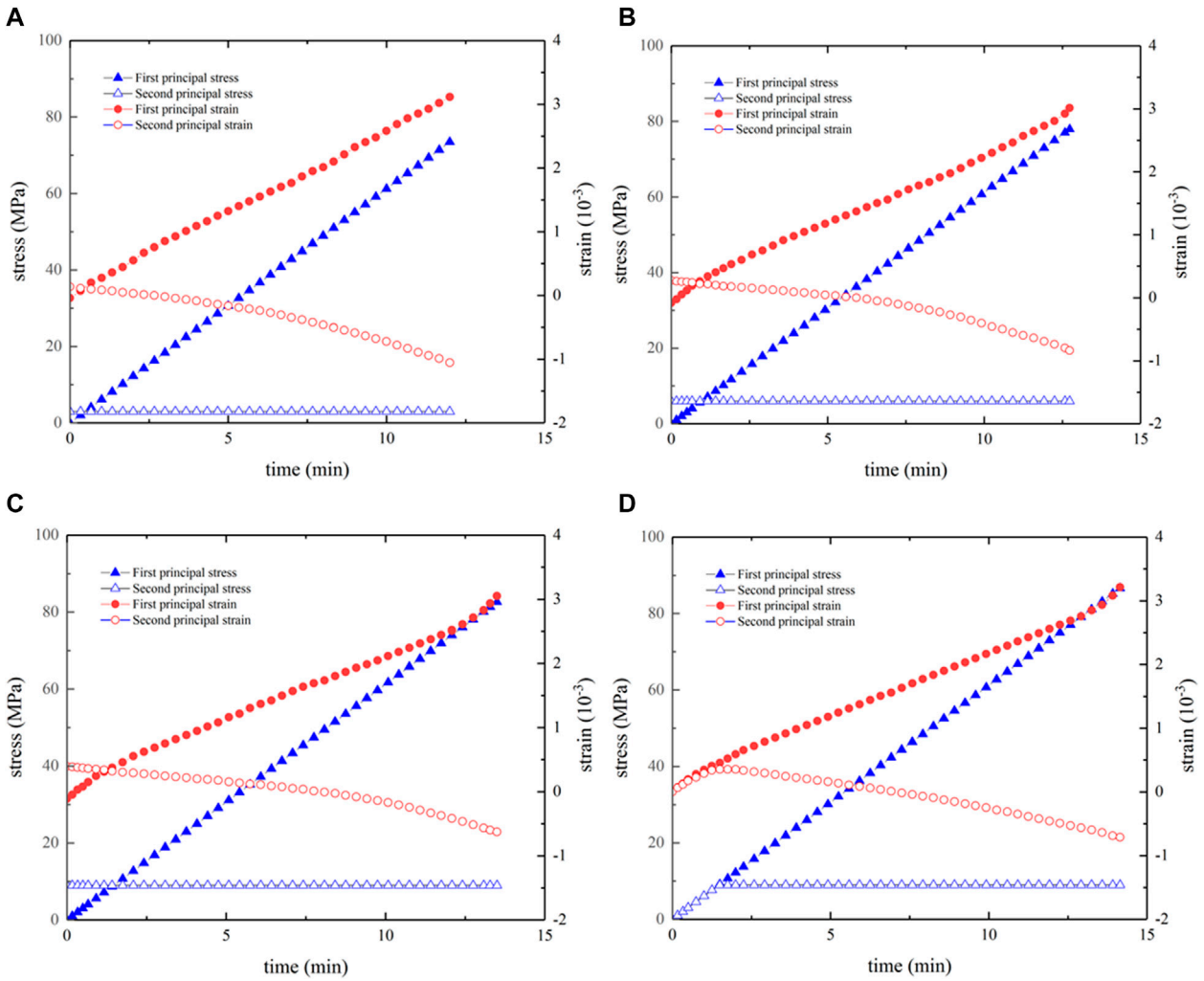

FIGURE 2 | Stress-strain-time curves for different loading paths under biaxial compression experiments.

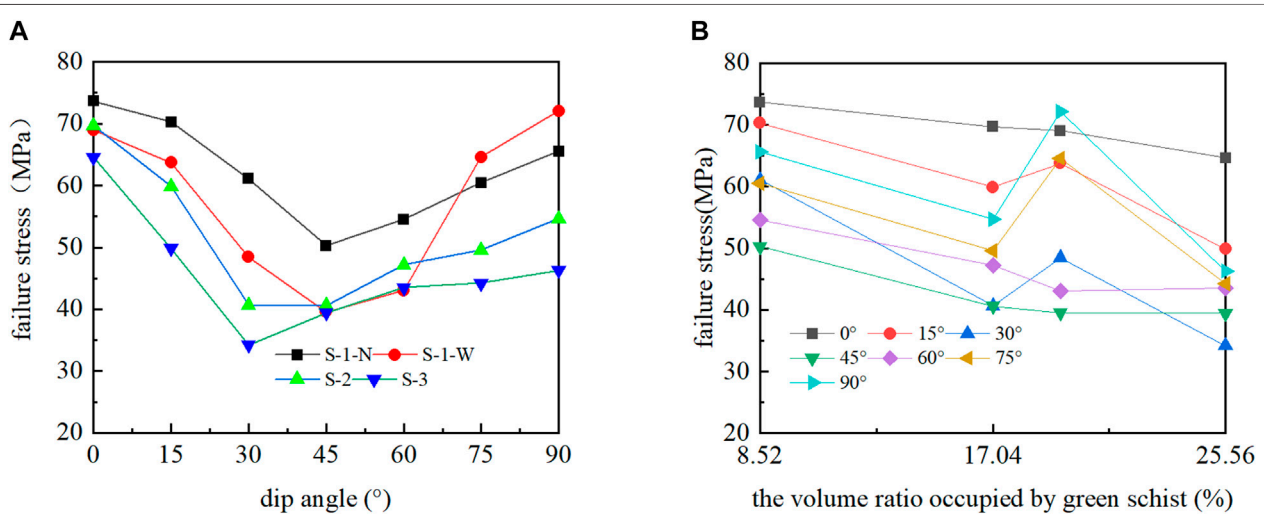

FIGURE 3 | Variation of the failure stress with the dip angle and the volume ratio occupied by green schist.

intermediate principal stress σ_2 increases from 3 MPa, 6–9 MPa. And the ultimate strain tends to increase as the intermediate principal stress σ_2 increases. At the intermediate principal stress $\sigma_2 = 9$ MPa, the first strain-time curve is more volatile in the first half for the constant lateral pressure loading path compared to the constant lateral pressure ratio followed by the constant lateral pressure loading path. This may be caused by the different timing of pore closure within the rock samples.

Figure 1E shows the failure pattern of typical 70 mm cubic rock samples under biaxial compression. It can be observed that the failure pattern under biaxial compression is basically the same as tension-shear failure. Spalling failure caused by tensile strain due to biaxial compression occurs first on the free surface of the rock samples. Afterward, as the loading continues to be applied, the tension failure of the rock sample gradually increases and the strength of the rock sample continues to weaken. Eventually, a shear failure surface is formed, leading to overall penetration failure. The cracks produced by tensile failure are mostly parallel to the vertical loading, and the main shear failure plane is basically an "X" shaped conjugate plane.

3.2 Numerical Results and Analysis

Figure 3 shows the variation of the failure strength corresponding to the test group S-1-N-β, S-1-W-β, S-2-β, and S-3-β with the dip angle and the volume ratio occupied by green schist. As can be seen from **Figure 3A**, the strength anisotropy of numerical samples in the four group tests is significant, and the failure strength-dip angle curve appears a parabolic-like concave shape, which is consistent with the U-shaped strength law of stratified rocks summarized by Hudson et al. (1993). With the same number of weak layers, test group S-1-W-β, where the percentage of volume of green schist is larger, has a smoother failure strength-dip angle curve than test group S-1-N-β. In terms of extremes, the minimum of failure strength for four group of tests occur between 30° and 60°, which is similar to the findings of Tien et al. (2001) and Mao et al. (2005), that is, the strength of soft-hard interbedded rock mass is higher and the failure is generally unaffected by the dip angle in the slow dip phase. However, as the dip angle increases the strength of the rock mass gradually decreases, tending to have a minimum at the middle dip angle phase. At the same time, a comparison shows that as the number of weak layers increases, the minimum tends to move forward, that is, when the number of weak layers is 2 and 3, the minimum of failure strength moves from 45° when the number of weak layers is 1 to near 30°.

As seen in **Figure 3B**, the failure strength shows an overall decreasing trend with the increase of the volume ratio occupied by green schist in the test groups with different dip angles, although there is a certain degree of fluctuation in individual cases. When the volume ratio occupied by green schist is close, the effect of increasing number of weak layers on the decrease of failure strength of rock samples has a positive correlation with the dip angle. It is also worth mentioning that the effect of the volume ratio occupied by green schist on the failure strength is greater in the range of medium to high level of dip angle for the weak layer number of 1.

4 CONCLUSION

(1) There is a significant difference in the failure pattern of rock samples in uniaxial and biaxial compression experiments. In uniaxial compression, the failure is usually in the form of splitting or shear failure, and in biaxial compression, spalling is first produced at the free surface due to tensile strain, and finally the shear failure is formed at an angle to the loading.
(2) In the biaxial compression experiment, the failure loading increases with the increasement of intermediate principal stress, and the first strain-time curve is more volatile in the first half for the constant lateral pressure loading path compared to the constant lateral pressure ratio followed by the constant lateral pressure loading path, which may be caused by the different timing of pore closure within the rock samples.
(3) The numerical results indicate that the number of weak layers has no significant effect on the U-shaped strength pattern of the soft-hard interbedded rock mass. However, with the increase of the number of weak layers, the minimum of the failure strength tends to move forward in the direction of the smaller dip angle; the failure loading shows an overall decreasing trend with the increase of the volume ratio occupied by green schist. And when the volume ratio occupied by green schist is close, the influence of increasing number of weak layers on the decrease of failure loading of rock samples is basically positively correlated with the dip angle.

DATA AVAILABILITY STATEMENT

The original contributions presented in the study are included in the article/Supplementary Material; further inquiries can be directed to the corresponding author.

AUTHOR CONTRIBUTIONS

All authors listed have made a substantial, direct, and intellectual contribution to the work and approved it for publication.

FUNDING

This work was supported by the National Natural Science Foundation of China (grant number 41672257), Fundamental Research Funds for the Central Universities (grant number B200202051), and Science and Technology Project of Zhejiang Provincial Transportation Department (grant number 2020014).

REFERENCES

Brady, B., and Brown, E. (2004). *Rock Mechanics for Underground Mining*. 3rd Edition. Springr.NY, USA.

Cazacu, O., Cristescu, N. D., and Shao, J. F. (1998). A New Failure Criterion for Transversely Isotropic Rocks. *Int. J. Rock Mech. Min. Sci.* 35 (5), 421. doi:10.1016/s0148-9062(98)00145-4

Chen, Z. J., and Zhuo, J. S. (2000). Application of "Sample Element Method" to Determination of Mechanical Parameters of Stratified Crack Rock Mass. *J. Hohai Univ. Nat. Sci.* 1(1), 16–19. (in Chinese). doi:10.3321/j.issn:1000-1980.2000.01.003

Chengdu Hydroelectric Investion, and (2003). *Teresearch Report of Check of Dam Site of Jinping I Hydropower Station at Yalong River (3): Engineering Geology Condition*. Chengdu, China: Chengdu Hydroelectric Investigation and Design Institute, China Hydropower Engineering Consulting Group Co. (in Chinese).

Deng, R. G., and Zhang, Y. (2001). On the Microstructure and Mechanical Properties of Greenschist in the Dam Site of Jinping Hydropower Station. *J. Chengdu Univ. Technol.* 28 (01), 93–97. (in Chinese). doi:10.3969/j.issn.1671-9727.2001.01.019

Duveau, G., and Shao, J. F. (1998). A Modified Single Plane of Weakness Theory for the Failure of Highly Stratified Rocksfied Single Discontinuity Theory for the Failure of Highly Stratified Rocks. *Int. J. Rock Mech. Min. Sci.* 35 (6), 807–813. doi:10.1016/s0148-9062(98)00013-8

Huang, S. L., Xu, J. S., Ding, X. L., and Wu, A. Q. (2010). Study on Layered Rockmass Composite Model Based on Characteristics of Structural Plane and its Application. *Chin. J. Rock Mech. Eng.* 29 (4), 743–756. (in Chinese).

Huang, S. L. (2008). *Study of Mechanical Model of Brittle Rock under High Stress Condition and its Engineering Applications*. Wuhan, China: PhD thesis, University of Chinese Academy of Sciences. (in Chinese).

Hudson, J. A. (1993). Comprehensive Rock Engineering. *Fundamentals*, 1. 1.

Jaeger, J. C. (1960). Shear Failure of Anistropic Rocks. *Geol. Mag.* 97, 65–72. doi:10.1017/s0016756800061100

Li, Y., Liu, W., Yang, C., and Daemen, J. J. K. (2014). Experimental Investigation of Mechanical Behavior of Bedded Rock Salt Containing Inclined Interlayer. *Int. J. Rock Mech. Min. Sci.* 69, 39–49. doi:10.1016/j.ijrmms.2014.03.006

Li, A., Shao, G. J., Su, J. B., Sun, Y., Yu, T. T., and Shi, H. G. (2018). Influence of Heterogeneity on Mechanical and Acoustic Emission Behaviours of Stratified Rock Specimens. *Eur. J. Environ. Civ. Eng.* 22 (S1), 381–414. doi:10.1080/19648189.2017.1373709

Lu, G.-y., Zhu, Z.-q., Liu, Q.-y., and He, X.-q. (2009). Failure Mode and Strength Anisotropic Characteristic of Stratified Rock Mass under Uniaxial Compressive Situation. *J. Cent. South Univ. Technol.* 16, 663–668. doi:10.1007/s11771-009-0110-7

Mao, H. J., and Yang, C. H. (2005). Study on Effects of Discontinuities on Mechanical Characters of Slate. *Chin. J. Rock Mech. Eng.* 24 (20), 53–58. doi:10.3321/j.issn:1000-6915.2005.20.008

Mclamore, R., and Gray, K. E. (1967). The Mechanical Behavior of Anisotropic Sedimentary Rocks. *J. Eng. Ind. Trans. ASME* 89, 62–73. doi:10.1115/1.3610013

Mohamed, I., and Heinz, K. (2019). Constitutive Model for Inherent Anisotropic Rocks: Ubiquitous Joint Model Based on the Hoek-Brown Failure Criterion. *Comput. Geotechnics* 105, 99–109. doi:10.1016/j.compgeo.2018.09.016

Niandou, H., Shao, J. F., Henry, J. P., and Fourmaintraux, D. (1997). Laboratory Investigation of the Mechanical Behaviour of Tournemire Shale. *Int. J. Rock Mech. Min. Sci.* 34, 3–16. doi:10.1016/s1365-1609(97)80029-9

Nova, R. (1980). The Failure of Transversely Isotropic Rocks in Triaxial Compression. *Int. J. Rock Mech. Min. Sci. Geomechanics Abstr.* 17 (6), 325–332. doi:10.1016/0148-9062(80)90515-x

Parisio, F., and Laloui, L. (2018). On the Formulation of Anisotropic-Polyaxial Failure Criteria: a Comparative Study. *Rock Mech. Rock Eng.* 51 (2), 479–489. doi:10.1007/s00603-017-1330-z

Pietruszczak, S., Lydzba, D., and Shao, J. F. (2002). Modelling of Inherent Anisotropy in Sedimentary Rocks. *Int. J. Solids Struct.* 39 (3), 637–648. doi:10.1016/s0020-7683(01)00110-x

Shen, P., Tang, H., Zhang, B., Ning, Y., and He, C. (2021). Investigation on the Fracture and Mechanical Behaviors of Simulated Transversely Isotropic Rock Made of Two Interbedded Materials. *Eng. Geol.* 286, 106058. doi:10.1016/j.enggeo.2021.106058

Tien, Y. M., and Kuo, M. C. (2001). A Failure Criterion for Transversely Isotropic Rocks. *Int. J. Rock Mech. Min. Sci.* 38 (3), 399–412. doi:10.1016/s1365-1609(01)00007-7

Tien, Y. M., and Tsao, P. F. (2000). Preparation and Mechanical Properties of Artificial Transversely Isotropic Rockficial Transversely Isotropic Rock. *Int. J. Rock Mech. Min. Sci.* 37, 1001–1012. doi:10.1016/s1365-1609(00)00024-1

Tien, Y. M., Kuo, M. C., and Juang, C. H. (2006). An Experimental Investigation of the Failure Mechanism of Simulated Transversely Isotropic Rocks. *Int. J. Rock Mech. Min. Sci.* 43, 1163–1181. doi:10.1016/j.ijrmms.2006.03.011

Wang, Z. C., Zong, Z., Qiao, L. P., and Li, W. (2018). Elastoplastic Model for Transversely Isotropic Rocks. *Int. J. Geomechanics* 18 (2), 1–15. doi:10.1061/(asce)gm.1943-5622.0001070

Xu, D.-P., Feng, X.-T., Chen, D.-F., Zhang, C.-Q., and Fan, Q.-X. (2017). Constitutive Representation and Damage Degree Index for the Layered Rock Mass Excavation Response in Underground Openings. *Tunn. Undergr. Space Technol.* 64, 133–145. doi:10.1016/j.tust.2017.01.016

Yan, P., Lu, W., He, Y., Zhou, W., Chen, M., and Wang, G. (2016). Coring Damage Mechanism of the Yan-Tang Group Marble: Combined Effect of Stress Redistribution and Rock Structure. *Bull. Eng. Geol. Environ.* 75 (4), 1701–1716. doi:10.1007/s10064-015-0842-6

Conflict of Interest: JL was employed by Pumped-storage Technology and Economic Research Institute State Grid Xin Yuan Company Ltd.

The remaining authors declare that the research was conducted in the absence of any commercial or financial relationships that could be construed as a potential conflict of interest.